The American Journal of Human Genetics, Volume *95*

Supplemental Data

CCDC151 Mutations Cause Primary Ciliary Dyskinesia by Disruption of the Outer Dynein Arm Docking Complex Formation

Rim Hjeij, Alexandros Onoufriadis, Christopher M. Watson, Christopher E. Slagle, Nikolai T. Klena, Gerard W. Dougherty, Małgorzata Kurkowiak, Niki T. Loges, Christine P. Diggle, Nicholas F.C. Morante, George C. Gabriel, Kristi L. Lemke, You Li, Petra Pennekamp, Tabea Menchen, Franziska Konert, June Kehlet Martin, Dorus A. Mans, Stef J.F. Letteboer, Claudius Werner, Thomas Burgoyne, Cordula Westermann, Andrew Rutman, Ian M. Carr, Christopher O'Callaghan, Eduardo Moya, Eddie M.K. Chung, UK10K, Eamonn Sheridan, Kim G. Nielsen, Ronald Roepman, Kerstin Bartscherer, Rebecca D. Burdine, Cecilia W. Lo, Heymut Omran, and Hannah M. Mitchison

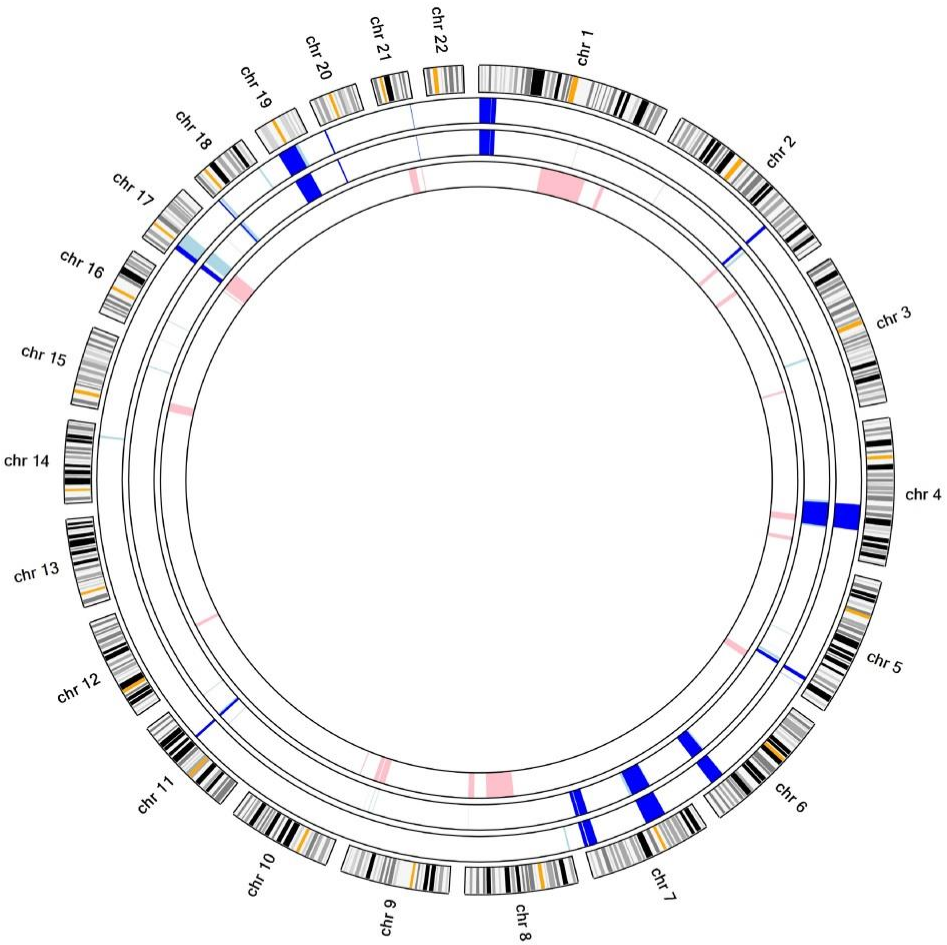

Chromosome	Start	End	Interval size (bp)
1	554,484	16,731,510	16,177,026
1	17,295,679	23,885,498	6,589,819
2	175,624,107	180,047,908	4,423,801
4	114,120,520	149,993,092	35,872,572
5	155,935,708	160,914,508	4,978,800
6	132,508,426	152,540,278	20,031,852
7	38,119,969	67,702,531	29,582,562
7	140,159,721	152,350,013	12,190,292
7	153,696,994	158,811,981	5,114,987
11	83,296,734	86,955,572	3,658,838
17	14,005,439	21,147,404	7,141,965
18	2,305,761	4,460,922	2,155,161
19	9,297,273	35,843,086	26,545,813
20	1,669,250	3,870,124	2,200,874
21	43,504,228	43,969,714	465,486

Figure S1. Autozygosity mapping in family 71154. A MultiIdeogram graphical plot of SNP (Affymetrix Genome-Wide Human SNP Array v6.0) versus exome data shows an autozygosity mapping output indicating regions of homozygosity on each chromosome. The image shows the chromosomes alongside SNP array data for the affected sibling 71154 II:2 (outer circle), exome data from the affected sibling (middle circle) and SNP array data from the unaffected sibling 71154 II:1 (inner circle). Regions of homozygosity are shown in light blue for the affected and pink for the unaffected. Dark blue shows homozygous regions shared across both data types in the affected, that are not present in the unaffected sibling, including a large region on chr19 spanning the *CCDC151* gene. Co-ordinates of the 15 dark blue autozygous regions identified as present in the affected but not unaffected sibling are shown in **Table S2**.

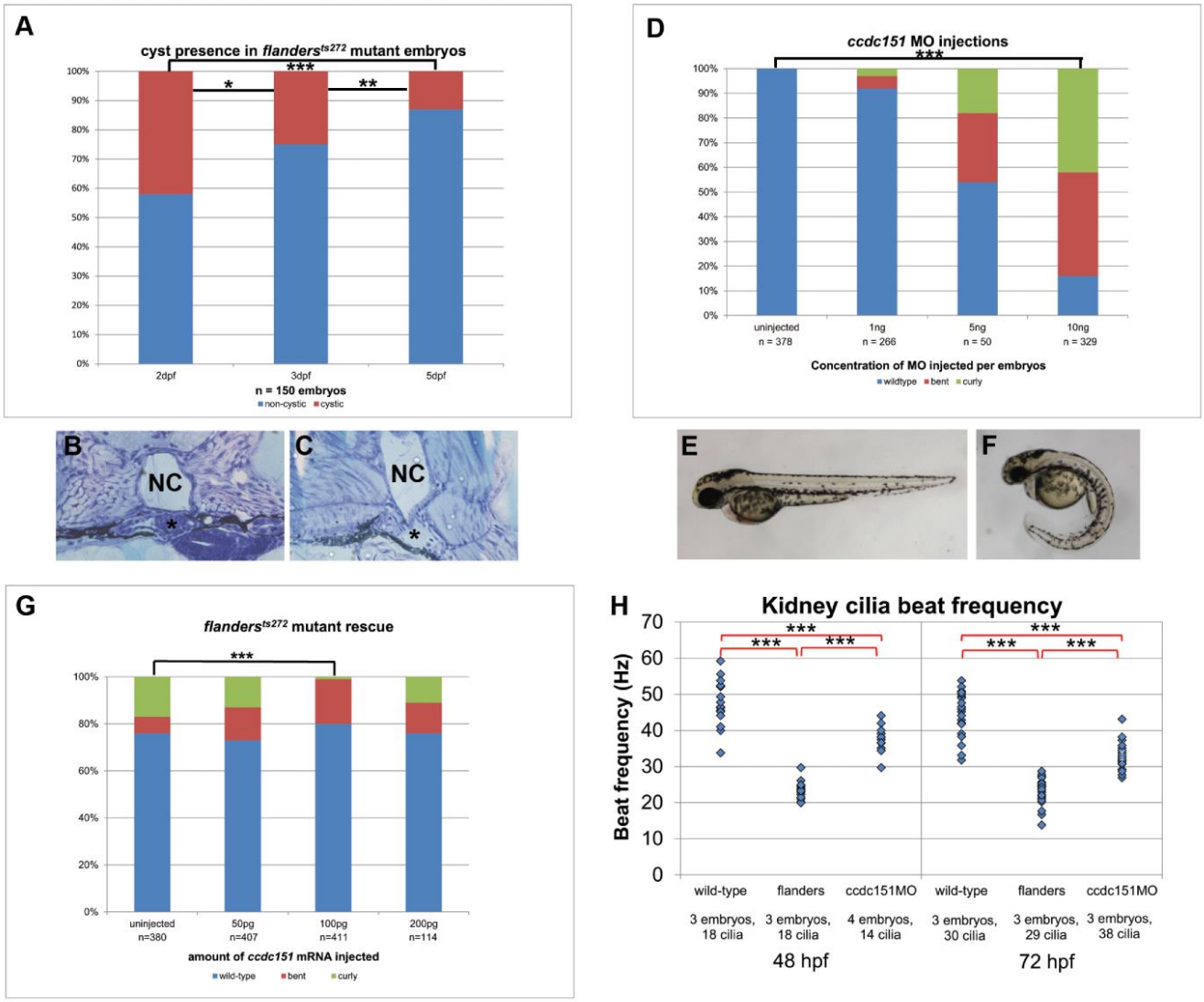

Figure S2. Additional characterization of *flanders*^{ts272} mutants and *ccdc151* morpholino injected embryos. (**A**) Frequency of pronephric cysts in *flanders* mutants. 150 mutant embryos, identified by the tail curl phenotype, were scored on three consecutive days for the presence of pronephric cysts. Pronephric cysts were qualitatively smaller than those we observe in mutants that more severely disrupt cilia motility. Cyst presence diminished over time suggesting that the cysts could resolve in the mutant embryos. chi-squared p-value * 0.002 between day 1 and 2, ** 0.005 between day 2 and 3, and *** $<10^{-8}$ between day 1 and 3. (**B**) Cross section of a wildtype sibling and (**C**) a *flanders* mutant kidney cyst. The glomerulus (asterisk) lies underneath the notochord (NC) and is dilated in mutant embryos. (**D**) Injection of a splice-blocking *ccdc151* morpholino can phenocopy the tail curl observed in *flanders* mutants producing tight curled tails (**F**) or tails with a slightly less pronounced curl (bent; not shown). Compare these phenotypes to those observed in **E** (uninjected). These phenotypes are dose dependent. *** chi-squared p-value $<10^{-114}$ (**G**) The tail curl observed in *flanders*^{ts272} mutant embryos can be partially rescued by injection of 100pg of *ccdc151* RNA per embryo. Higher and lower concentrations were not as effective at rescuing the tail curl phenotype. RNA was injected into clutches of embryos from *flanders*$^{ts272/+}$ heterozygote parents. Thus 25% of the embryos are expected to be *flanders*^{ts272} mutants. *** chi-squared p-value $<10^{-16}$ (**H**) Quantification of pronephric cilia beat frequency in *flanders* mutants, *ccdc151* morpholino (MO) injected and siblings at 48hpf and 72hpf. *** student's t-test p-value $< 10^{-16}$. Data from Figure 2 is reproduced here for comparison. The morpholino injected embryos displayed slightly higher beat frequencies compared to *flanders* mutants, yet morpholino injected embryos still had reduced frequencies compared to wild-type embryos.

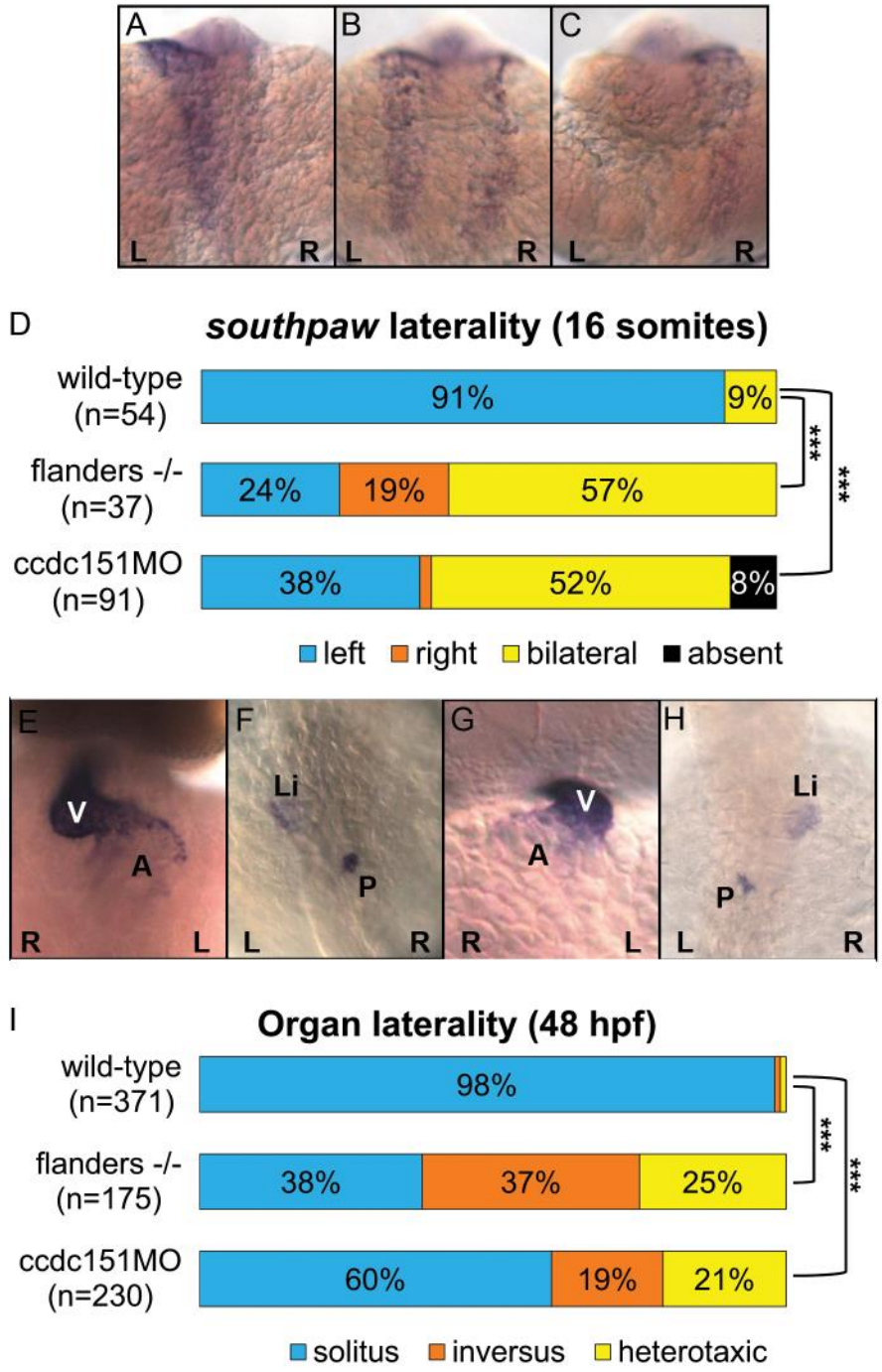

Figure S3. Left-right patterning defects observed in *flanders*^{ts272} mutants and *ccdc151* morpholino injected embryos. Representative embryos expressing *southpaw* by *in situ* hybridization on the (**A**) left, (**B**) both sides, or (**C**) right within the lateral plate mesoderm of 16 somite embryos. (**D**) Quantification of *southpaw* expression patterns in wild-type versus *flanders* mutants and *ccdc151* morpholino injected embryos. Data from Figure 2 is reproduced here for comparison. *** chi squared p-value < 10^{-9} (**E-H**) *in situ* hybridization to visualize the heart (*myl7*), pancreas (*insulin*) and liver (*fkd2*) as described[48]. In wild-type embryos the heart (E; ventral view) loops to the right placing the ventricle (V) to the right of the atrium (**A**). (F; dorsal view) the liver (Li) is on the left and the pancreas (P) is on the right. In *flanders* mutants and *ccdc151* morpholino injected embryos, the heart and viscera can be reversed (*situs inversus*) as shown in the embryo pictured in (**G**) and (**H**), or heterotaxic referring to a randomized positioning of these organs with respect to one another. (**I**) Quantification of organ laterality in wild-type versus *flanders* mutants and *ccdc151* morpholino injected embryos. Data from Figure 2 is reproduced here for comparison. *** chi-squared p-value < 10^{-55}. Left (L) and right (R) are indicated.

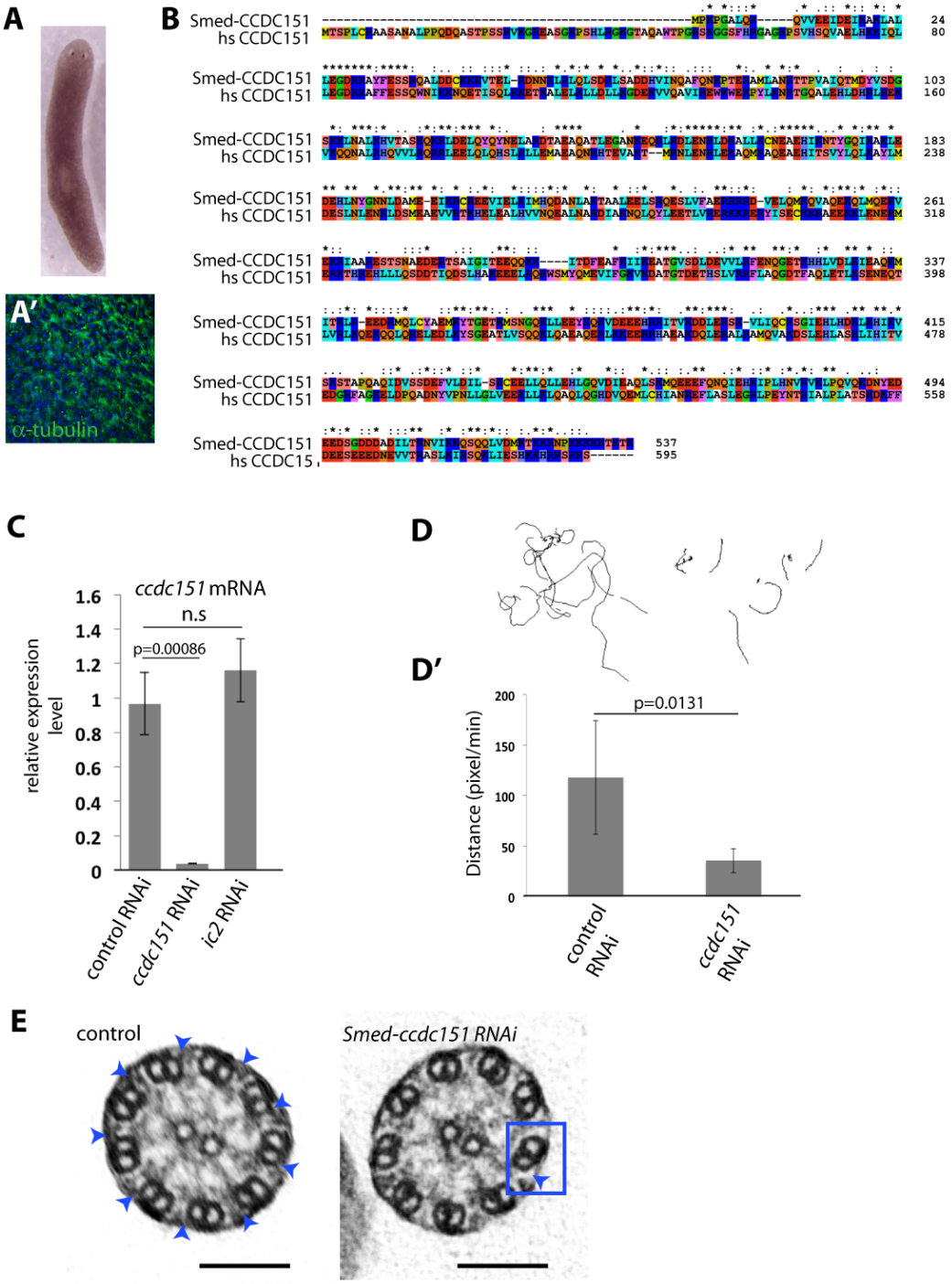

Figure S4. A putative *ccdc151* ortholog (*Smed-ccdc151*) is required for cilia-mediated locomotion in the planarian species *Schmidtea mediterranea*. (**A**) Planarians (adult *Schmidtea mediterranea*) in (A)) move on ventral cilia, which can be visualized with an antibody against acetylated alpha-tubulin (A'). (**B**) Alignment of *Smed*-CCDC151 with human CCDC151 using ClustalX (http://www.clustal.org). Amino acids with similar properties are color-coded by similar colors. Planarian flatworms of the species *Schmidtea mediterranea* (Clonal Line BCN-10) were kept in the dark in plastic tanks filled with artificial water at 19°C. The water was changed twice a week and planarians were fed once a week with calf liver. Animals were starved 7 days prior RNAi experiments. RNAi was performed as previously described[46]. dsRNAs against green fluorescent protein mRNA (*gfp*) and *Smed-ic2* mRNA[47] were used as controls. The locomotion phenotype observed after *Smed-ccdc151* RNAi was confirmed with two independent dsRNAs. Primer sequences are listed below. To extract total RNA we used TRIzol reagent (Invitrogen) and cDNA was synthesized using RevertAid First Strand cDNA Synthesis Kit (Thermo Scientific). Quantitative PCR reactions were performed

using the TaqMan Universal PCR Master Mix (Applied Biosystems) and knockdown efficiency was determined using the Real-Time PCR System 7500 (Applied Biosystems). Three biological replicates were measured in duplicates. *Gapdh* was used as reference gene. Primer sequences are listed below. (**C**) Quantitative real-time PCR analysis of *Smed-ccdc151* mRNA expression levels after *gfp* (control), *Smed-ic2*, or *Smed-ccdc151* RNAi. *Smed-ccdc151* expression levels are strongly reduced after *ccdc151* RNAi but not after RNAi of the control genes *gfp* or *Smed-ic2*. Error bars represent standard deviations of the mean of three biological replicates. (**D, D'**) Locomotion assay with *gfp* and *Smed-ccdc151* RNAi animals quantifying traveled distance (D') where 3x 10 animals were scored, and representative paths travelled by 10 animals (D). We used the Intas iX UV-Gel-Imager to take sequential Pictures (1 picture per second for 1 min) of RNAi animals. The animals were placed in the center of a container covered with a minimal volume of water with their dorsal side up. Images were analyzed with Fiji. (**E**) TEM analysis shows a loss of outer dynein arms in *Smed-ccdc151* RNAi compared to controls. Scales bars, 0.1µm.

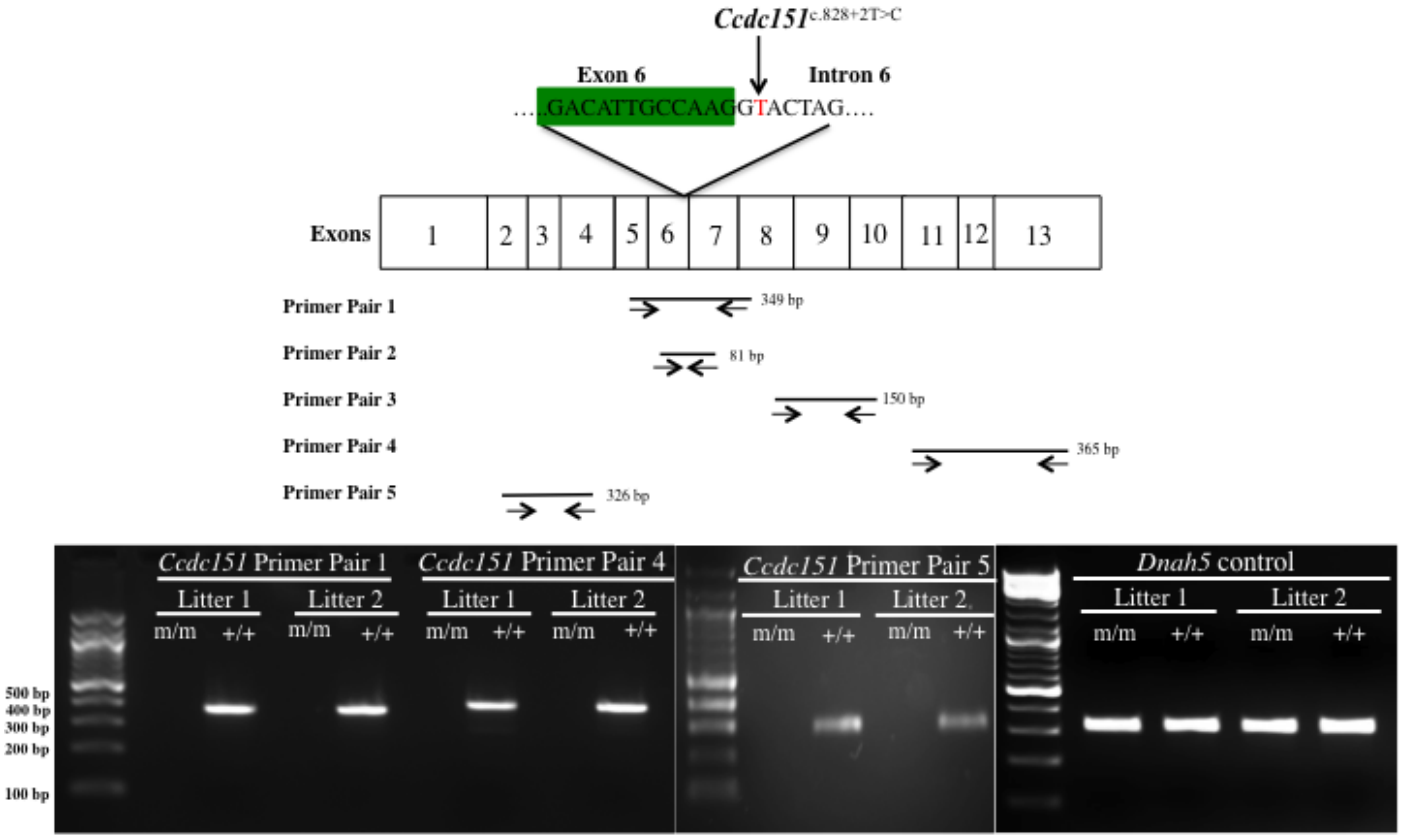

Figure S5. RT-PCR confirmation of splice defect in *Ccdc151*^{snbl} mice. Total RNA was isolated from trachea of *Ccdc151*^{snbl} mice and control littermates using the RNeasy Plus Micro Kit (Qiagen). cDNA was synthesized from total RNA and PCR amplified using AmpliTaq Gold™ DNA polymerase (Life Technologies) using cycle parameters: 95°C for 5 min, followed by 40 cycles at 95°C for 30 s, 58°C for 30 s and 72°C for 1 min, then 72°C for 5 min. Five primer pairs were used for PCR amplification to interrogate the *Ccdc151* transcript, and *Dnah5* was also amplified as a positive control (All primers listed in Table S1).

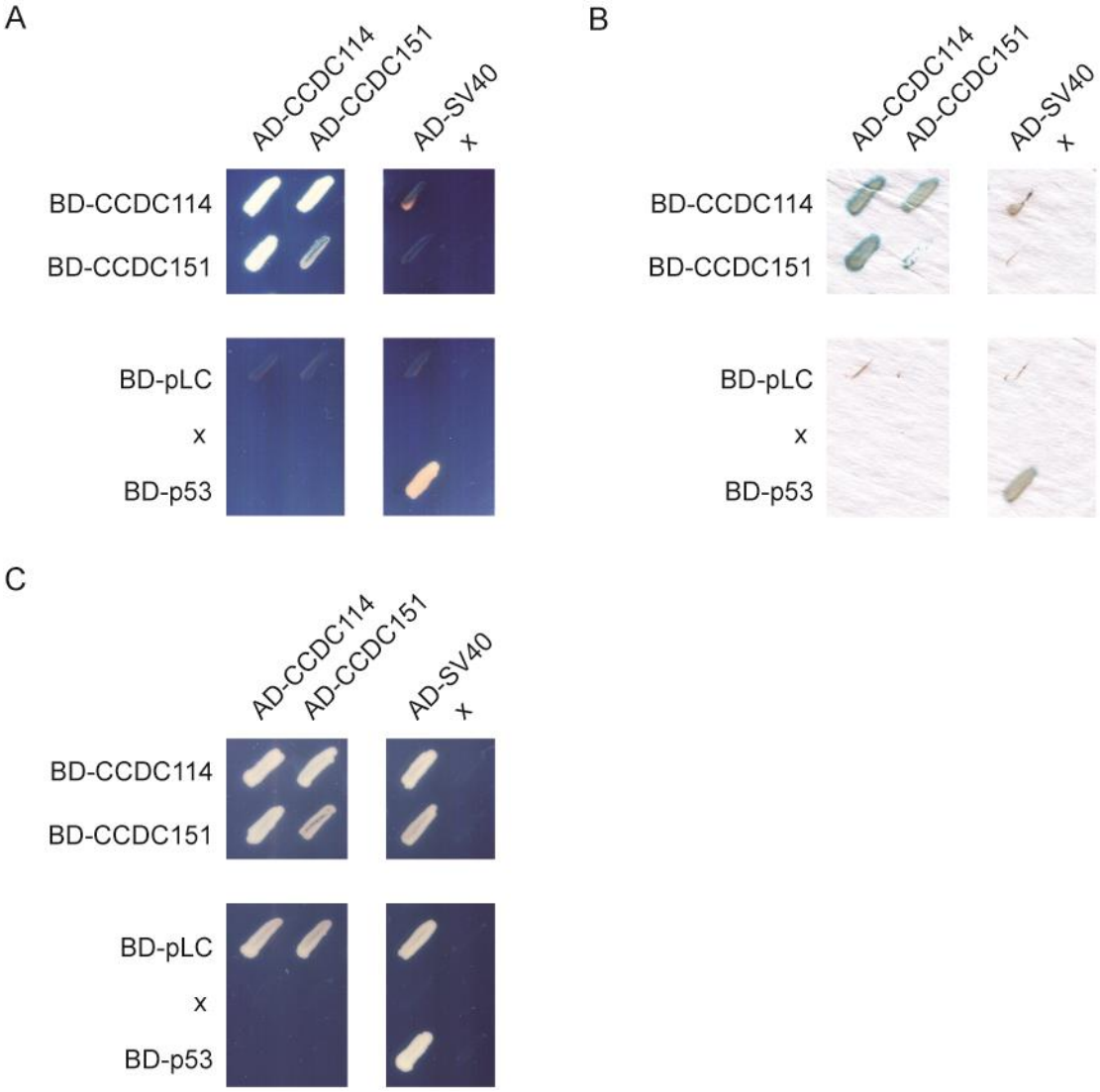

Figure S6. Binary interaction between CCDC151 and CCDC114. Yeast two-hybrid screening of CCDC151 and CCDC114 reveals direct protein interaction between CCDC151 and CCDC114. Plasmids expressing full-length CCDC151 and CCDC114 were fused to a DNA-binding domain (GAL4-BD) or to an activation domain (GAL4-AD), transformed in yeast strains PJ69-4A and PJ69-4α respectively, and subsequently combined by yeast mating. Diploids containing both plasmids were selected in media lacking leucine and tryptophane (SD-LW; panel C). Interactions were analyzed by assessment of reporter gene (*HIS3* and *ADE2*) activation via growth on selective media (SD-LWAH; panel A) and β-galactosidase colorimetric filter lift assays (*LacZ* reporter gene; panel B). As a positive control, the binding capacity of BD-p53 and SV40-AD was assessed; as negative controls, BD-pLC and AD-SV40, which thus far have not been associated with either CCDC151 or CCDC114, were included in this assay.

Table S1. Miscellaneous primers used in this study

	Forward	**Reverse**
Flanders	GGGACAGCATGCCAAACTTGCTTATAATCAATC	CTTGGCAGCATCCTTAGACAGATGAGC
Schmidtea		
dsRNA		
Smed-ic2	GGGAATTAATCATACCGAAG	CATCCCAATGTATGAATCTG
Smed-ccdc151	CGAACTAGCTAGAGATACGC	ACACAAACTTTCTTGACGTG
qPCR		
CCDC151 (probe*:* UPL143)	Ttggccaagttgacattgaa	Gacattgtgaagcggaatttt
GAPDH (probe*:* UPL68)	CATCAAAATTGTGGAGAGATGG	CCAGTTGAAGCCGGAATAAT
***Ccdc151*^{SnbI}**		
primer pair 1	TGCGCAACCTGGAGAATCGGC	CTCCATACGCTCTGTCTGAA
primer pair 2	AGTGAATCAAGAGGCTATAA	CGATCTCTGATCGCAGACTC
primer pair 3	TAGTGCGCAGGTTCCTGGCG	CGTGGAGCCTCCGCTGGCTCA
primer pair 4	TGATACGGTATTGGCAGGAA	TAAGATCTGCGCAACCTATT
primer pair 5	GAGAGCTCCCAATGGAACAT	TCTTGGACCTCTGCCATCTC
Dnah5	TGAGCTTTAACACGTTAGACACG	TCAGACTGTTCTGTGCACCTG
cDNA cloning		
CCDC114-UTR pDONR201-*CCDC114*	5'UTR-F: GAGCGAGACCCTGTCTAGAAAAA GGGGACAAGTTTGTACAAAAAAGCAGGCTTCatg gaaggggagaggcgggcctac	3'UTR-R: GAACAGGAGATCAGGAGTCAGAG GGGGACCACTTTGTACAAGAAAGCTGGGTTTAgcccc gggagtctttgctggtggag
CCDC151-UTR pDONR201-*CCDC151*	5'UTR-F: TAACCCCTAGGGGCCTTCAGCCC GGGGACAAGTTTGTACAAAAAAGCAGGCTTCatg acatctcctctgtgcagggcg	3'UTR-R: GGTAACATTTATTGCGCAACTCTGAGGCC GGGGACCACTTTGTACAAGAAAGCTGGGTTTAggacc tccgagagcgacggtgcttc

For dsRNA synthesis the T7 polymerase promoter sequence (TAATACGACTCACTATAGGG) was attached to the 5'-ends of forward and reverse primers. UPL numbers correspond to Roche Universal Probe Library probe numbers that were used to validate knockdown efficiency.

Table S2. Filtering process for gene variants identified through gene panel sequencing of UCL-65 II:8

	UCL-65 II:8
Total variants in gene panel	5,378
Variants in MAF<0.01 in 1000 genomes	584
Heterozygous variants	392
Heterozygous nonsynonymous, splice-site, or insertion/deletion variants	59
Genes with compound heterozygous variants	4 (*MLL3, PCSK5, DCHS1, DNAH2*)
Of these, genes with compound heterozygous variants, and predicted to have motile ciliary functions	1 (*DNAH2*); 3 heterozygous variants: (1) rs149406306: c.11899C>T, p.Pro3967Ser (benign) (2) c.3481C>A, p.Arg2738Gln (benign) (3) rs7601298: c.6226T>C, p.Ser2076Pro (rare, probably damaging, 0.97)
Homozygous variants	190
Homozygous nonsynonymous, splice-site, or insertion/deletion variants	13 autosomal homozygous (*DNAH3, WNT2B, STAB2, NCOR2, DPF3, KRTAP9-1, KDM6B, CCDC40, CCDC151, KLHL23, MAML3, WDR27, PDHA1*) plus 4 x-linked hemizygous (*GPR112, IL1RAPL1, MXRA5, ATRX*)
Of these, genes with homozygous ORF-located variants, and predicted to have motile ciliary functions	3 homozygous variants (*DNAH3, CCDC40, CCDC151*): (1) *DNAH3* rs138753702: c.9881T>A, p.Tyr3294Phe (rare, possibly damaging, 0.837) (2) *CCDC40* rs10693712: c.3040-3041insCAC, p.Arg1014ThrArg (rare, in-frame single residue insertion, consequence unknown) *(3) CCDC151* c.925G>T, p.309* (unique, stop-gain)

MAF: Minor allele frequency; ORF: open reading frame. Variant pathogenic predictions were assessed according to GERP, PolyPhen2, SIFT, Condel; only the Polyphen2 score is displayed.

Table S3. Filtering process for gene variants identified through exome sequencing of 71154 II:2

	71154 II:2
Total variants in exome	31,964
Homozygous variants located in 14 autozygous regions totalling 174 Mb*	1,480
Variants with MAF <0.01 in exome variant server database or dbSNP 139	156
Splice-site, nonsynonymous or insertion-deletion variants	57
Variants in PCD candidate genes	1 (*CCDC151* c.1256C>T, p.Ser409*)

MAF: Minor allele frequency;
*Regions determined from combined SNP and exome data analysis of 71154 II:2 the proband and 71154 II:1 an unaffected sibling (shown in dark blue in Figure S1).

Table S4. Documented clinical features of individuals carrying *CCDC151* mutations

ID	Homozygous mutations	Sex	Age at diagnosis	Origin	TEM findings	Situs inversus	Neonatal respiratory distress syndrome	NO	LM	Documented bronchiectasis	Recurrent respiratory tract infections, chronic cough, wheeze, bronchitis	Sinusitis, rhinorrhea, nasal	Otitis media (OM) and hearing problems
OP-675	c.925G>T; p.Glu309*	M	16 years	Egypt	ODA defect	Situs inversus, cardiac ventricular septal defect	Yes	ND	Static	Yes	Chronic wet cough	Chronic sinusitis, chronic nasal obstruction	Normal hearing
OP-1255	c.925G>T; p.Glu309*	F	10 weeks	Egypt	ODA defect	Situs inversus	Yes, persistent tachypnea and desaturation below 90% from 2 days old.	9-11 ppb	Static	Yes	Recurrent respiratory tract infections	Nasal obstruction and chronic nasal secretions	Normal hearing
PCD-65 II:7	c.925G>T; p.Glu309*	F	1 year	Arabic-Bedouin	ODA defect	Dextrocardia, abdominal situs inversus	Yes	ND	Static	ND	Pneumonia, recurrent productive cough, wheezing, bronchitis. Asthma.	Chronic sinusitis	Conductive hearing loss, OM and effusions
PCD-65 II:8	c.925G>T; p.Glu309*	M	6 years	Arabic-Bedouin	ODA defect	Situs solitus	Yes, symptoms from birth	ND	Static	ND	Pneumonia, recurrent productive cough		OM and effusions
71154 II:2	c.1256C>T; p.Ser419*	M	12 years	Pakistan	ODA defect	Dextrocardia, abdominal situs inversus	No	ND	Static	infiltrate/atelectasis in x-ray	Recurrent respiratory symptoms presumed to be asthma	Nasal polyps, chronic pansinusitus, runny blocked nose	

M: Male; F: Female; TEM: Transmission electron microscopy; ODA: Outer dynein arm; NO: Nitric oxide; ND: Not determined; LM: Light microscopy; CBF: Ciliary beat frequency

Table S5. Recovery of Disease Causing *Ccdc151* Mutation in *Snowball* Mutant

	***Snowball* mutant (1885-004-LA)**
Average Coverage	51.8x
Total variants	3,604
Novel coding variants	69
Novel homozygous coding variants	5 (1) *Ept1*: c.C356A, p.P119Q (2) *Atn1*: c.C1345T, p.R449C (3) *Epor*: c.A523G, p.T175A (4) *Ccdc151:* c.828+2T>C (5) *Plec*: c.G5074A, p.A1692T
Homozygous among all *snowball* mutants	1 (*Ccdc151*$^{c.828+2T>C}$)

Table S6. Cardiac defects documented in a panel of homozygous *Ccdc151*^{snbl} mutant mice

ID	Situs	Apex	Loop	Arch	Atria	OFT	Septal Defects	IVC	Van Praagh	Lung	Bronchial branching	Gut	Abdomen situs	Liver situs
1	HTX	Lev	D	Right	SS	Inv*	mVSD	Left	{S, D, S}	Norm (3R/2L)	Norm	Norm	Norm. L(st/Sp/P)	Norm (1R/2L)
2	HTX	Dex	L	Right	SI	Inv	mVSD	Dual	{I, L, I}	Inv (1R/3L)	Inv	Mal	Dsc. R(St/Sp) Mid (P)	Norm (1R/2L)
3	HTX	Lev	D	Left	SS	Norm	None	Right	{S, D, S}	Norm (3R/2L)	Norm	Norm	Inv. R(St/Sp/P)	Inv (2R/1L)
4	HTX	Dex	L	Right	ND	Inv	ND	Left	{I, L, I}	Inv (2R/3L)	ND	Norm	Inv. R(St/Sp/P)	RI (1L/1R)
5	HTX	Dex	L	Right	ND	Inv	ND	Dual	{I, L, I}	LI (1R/1L)	ND	Norm	Norm. L(St/Sp/P)	Nml (1R/2L)
6	SIT	Dex	L	Right	ND	Inv	ND	Left	{I, L, I}	Inv (2R/3L)	ND	Norm	Inv. R(St/Sp/P)	Inv (2R/1L)
7	SIT	Dex	L	Right	ND	Inv	ND	Left	{I, L, I}	Inv (2R/3L)	ND	Mal	Inv. R(St/Sp/P)	Inv (2R/1L)
8	SIT	Dex	L	Right	SI	Inv	None	Left	{I, L, I}	Inv (2R/3L)	Inv	Norm	Inv. R(St/Sp/P)	Inv (2R/1L)
9	SIT	Dex	L	Right	SI	Inv	None	Left	{I, L, I}	Inv (2R/3L)	Inv	Mal	Inv. R(St/Sp/P)	Inv (2R/1L)
10	SIT	Dex	L	Right	SI	Inv	None	Left	{I, L, I}	Inv (2R/3L)	Inv	Norm	Inv. R(St/Sp/P)	Inv (2R/1L)
11	SIT	Dex	L	Right	SI	Inv	None	Left	{I, L, I}	Inv (2R/3L)	Inv	Norm	Inv. R(St/Sp/P)	Inv (2R/1L)
12	SS	Lev	D	Left	ND	Norm	ND	Right	{S, D, S}	Norm (3R/2L)	ND	Norm	Norm. L(st/Sp/P)	Norm (1R/2L)
13	SS	Lev	D	Left	ND	Norm	ND	Right	{S, D, S}	Norm (3R/2L)	ND	Norm	Norm. L(st/Sp/P)	Norm (1R/2L)
14	SS	Lev	D	Left	ND	Norm	ND	Right	{S, D, S}	Norm (3R/2L)	ND	Norm	Norm. L(St/Sp/P)	Norm (1R/2L)
15	SS	Lev	D	Left	ND	Norm	ND	Right	{S, D, S}	Norm (3R/2L)	ND	Norm	Norm. L(St/Sp/P)	Norm (1R/2L)

Situs: HTX: Heterotaxy; SIT: *Situs inversus totalis*; SS: *Situs solitus*; **Apex (heart apex):** Lev: Levocardia; Dex: Dextrocardia; **Loop (heart looping):** D: D Loop; L: L Loop; **Atria:** SS: *Situs solitus*; SI: *Situs inversus totalis*; **OFT (cardiac outflow tract):** Inv: Inverted positioning; Norm: Normal positioning; Inv*: affects the major aortopulmonary collateral arteries (MAPCA) – this sample is missing left pulmonary artery, supply to lungs comes from the aorta; **Septal Defects:** mVSD: muscular ventricular septal defect; **IVC:** position of inferior vena cava; **Van Praagh:** Cardiac anatomy classification using a 3-part series of letters describing malorientation of the atria, ventricles, and great vessels respectively[1]. In brief, {S, D, S} indicates normal anatomy and {I, L, I} indicates heterotaxy/situs inversus; **Lung:** Norm: Normal lobation; Inv: Inverted lobation; R/L denotes number of right/left lobes; **Bronchial branching:** Norm: Normal branching; Inv: Inverted branching; **Gut:** Norm: normal looping; Mal: malrotation of the intestines; **Abdomen situs:** Norm: situs solitus positioning; Inv: situs inversus positing; Dsc: discordant positioning; **Liver situs:** Norm: Normal lobation; Inv: Inverted; StSpP: stomach, spleen, pancreas, either left (L) or right side (R); Mid: midline; lobation, R/L denotes number of right/left lobes.

Video legends

Video S1. Videomicroscopy showing dysmotile cilia in the Kupffer's vesicle of *flanders* (*ts272a*) mutant zebrafish

Video S2. Videomicroscopy showing motile cilia in the Kupffer's vesicle of control *flanders* unaffected sibling

Video S3. Videomicroscopy showing pronephric ciliary beat in unaffected embryos

Video S4. Videomicroscopy showing pronepric ciliary beat in *flanders* mutant. Cilia beat regularly with significantly reduced beat frequency.

Videos S5-S6. *ccdc151* RNAi planarians move by muscle contraction rather than gliding. Planarians were injected with dsRNAs either against gfp (control; **Video S5**) or *ccdc151* (**Video S6**). Videos were taken 14 days after the first dsRNA injection using a stereomicroscope (Leica M80 with Leica IC80 HD Camera).

Video S7. Videomicroscopy showing immotile cilia in the tracheal epithelia of *Ccdc151*^{Snbl} mutant
Videomicroscopy of tracheal airway epithelia from homozygous *Ccdc151*^{Snbl} mutant mice reveals immotile cilia, whereas littermate control mice show normal rapid synchronous ciliary beating.

Video S8. Videomicroscopy showing motile cilia dysfunction in ependymal cilia of *Ccdc151*^{Snbl} mutant
Videomicroscopy of brain tissue sliced from the third ventricle of newborn homozygote *Ccdc151*^{Snbl} mutant mice reveals mostly immotile cilia, with patches of cilia having slow and restricted ciliary motion. In contrast, ependymal cilia from littermate control mice show normal rapid synchronous ciliary beating.

Video S9. Visualisation of an apparent coronary fistula in a *Ccdc151*^{Snbl} mutant
A digital video recording of a *Ccdc151*^{Snbl} mutant shows the heart beating through its contractile cycle, with a coronary artery fistula delineating a longitudinal translucent dark red region in the ventricular septum (indicated by arrow). This was confirmed by histopathology examination (see **Figures 3D, VII, VIII and IX**).

Video S10. Analysis of ciliary beating pattern of respiratory cilia from OP-675 by high-speed videomicroscopy. The cilia are immotile.

Video S11. Analysis of ciliary beating pattern of respiratory cilia from OP-1255 by high-speed videomicroscopy. The cilia are immotile.

Video S12. Analysis of ciliary beating pattern of respiratory cilia from a control by high-speed videomicroscopy.

Supplemental references

1. Schallert, E.K., Danton, G.H., Kardon, R., and Young, D.A.(2013). Radiographics *33*, 33-46.